Early defects in translation elongation factor 1α levels at excitatory synapses in α-synucleinopathy

Sonja Blumenstock[1,2,7], Maria Florencia Angelo[3,4], Finn Peters[2], Mario M Dorostkar[1], Manja Luckner[5], Sophie Crux[2,7], Lenka Slapakova[1], Viktoria Ruf[1], Thomas Arzberger[1], Stéphane Claverol[6], Etienne Herzog*[3,4] and Jochen Herms*[1,2,7]

[1]Center for Neuropathology and Prion Research, Ludwig-Maximilians University, Munich, Germany.
[2]German Center for Neurodegenerative Diseases (DZNE), Munich, Germany.
[3]Université de Bordeaux, Interdisciplinary Institute for Neuroscience, UMR5297, F-33000 Bordeaux, France.
[4]CNRS, Interdisciplinary Institute for Neuroscience, UMR5297, F-33000 Bordeaux, France.
[5]Department of Biology I, Biozentrum Ludwig- Maximilians University, Munich, Germany.
[6]Plateforme Proteome, Centre Génomique Fonctionnelle de Bordeaux, Université de Bordeaux, Bordeaux, France.
[7]Munich Cluster of Systems Neurology (SyNergy), Munich, Germany.

*To whom correspondence should be addressed (authors contributed equally to this work):

etienne.herzog@u-bordeaux.fr
Phone: +33 (0) 5 33 51 47 79

jochen.herms@med.uni-muenchen.de
Phone: +49 (0) 89 / 4400-46427
Fax: +49 (0) 89 / 4400-46508

Abstract

Cognitive decline and dementia in neurodegenerative diseases is associated with synapse dysfunction and loss, which may precede neuron loss by several years. While misfolded and aggregated α-synuclein is recognized in the disease progression of synucleinopathies, the nature of glutamatergic synapse dysfunction and loss remains incompletely understood. Using fluorescence-activated synaptosome sorting (FASS), we enriched to unprecedented purity excitatory glutamatergic synaptosomes from mice overexpressing human alpha-synuclein (h-αS) and wild-type littermates. Subsequent label free proteomic quantification revealed a set of proteins differentially expressed upon human alpha-synuclein overexpression. These include overrepresented proteins involved in the synaptic vesicle cycle, ER-Golgi trafficking, metabolism and cytoskeleton. Unexpectedly, we found and validated a steep reduction of eukaryotic translation elongation factor 1 alpha (eEF1A1) levels in excitatory synapses, at early stages of h-αS mouse model pathology. While eEF1A1 reduction correlated with the loss of postsynapses, its immunoreactivity was found on both sides of excitatory synapses. Finally, we observed a reduction in eEF1A1 immunoreactivity in the cingulate gyrus neuropil of patients with Lewy body disease along with a reduction in PSD95 levels. Altogether, our results provide a link between structural impairments underlying cognitive decline in neurodegenerative disorders and local synaptic defects. eEF1A1 may therefore represent a limiting factor to synapse maintenance.

Keywords: alpha-synuclein, elongation factor 1 alpha, synapse, proteomics, Lewy body dementia, FASS

Introduction

Since the description of alpha-synuclein (α-syn) as the major constituent of Lewy bodies [70], this protein has been in the focus for understanding the etiology of a group of diseases called synucleinopathies. Parkinson's disease (PD) is the most prominent member of this group which further includes Parkinson's disease dementia (PDD), dementia with Lewy bodies (DLB), multiple system atrophy (MSA) and some less well-characterized neuroaxonal dystrophies [80].

In neurons, α-syn is a component of synaptic vesicles and has been described as unfolded when soluble in the cytoplasm and forming α-helices when binding to curved membranes [6] and lipid rafts [5, 24, 27, 29]. α-syn influences synaptic vesicle clustering [24, 31, 67], exocytosis [48, 59, 67], endocytosis [81], and microtubule dynamics [15]. Nevertheless, the molecular mechanism responsible for the presynaptic (dys-)functions of α-syn remains poorly understood and the triggers for α-syn accumulation in synucleinopathies are not precisely known.

In a previous study, we have shown that the excess of α-syn causes destabilization and loss of dendritic spines in the mouse neocortex. Mice overexpressing α-syn under the PDGFβ promotor show high levels of cortical α-syn [2, 52] and spine loss months before any behavioral impairment [8]. Yet, the molecular changes underlying the observed synapse loss remained unknown. Therefore, we embarked on an unbiased mass spectrometry approach to analyze the relative protein composition between excitatory synapses of PDGF-h-αS and control mouse forebrains.

Due to the enormous complexity of brain tissue proteome [26, 40, 68] and the synaptic localization of α-synuclein [29, 49], a sample preparation that aims to reduce complexity and remove extra-synaptic peptides is mandatory. To that end, subcellular fractionation of intact synaptic compartments – termed synaptosomes – has been used [21, 34, 79]. Yet this type of

samples still suffer from the presence of a significant fraction of extra-synaptic material and all types of synapses regardless of their neurochemical nature [66]. We recently developed the fluorescence-activated synaptosome sorting (FASS) which allows the separation of specific synaptic subpopulations using a genetically encoded fluorescence reporter and a cell sorter [7, 50]. FASS purification of excitatory synaptosomes labeled with the vesicular glutamate transporter, VGLUT1^{venus} [39] depleted several hundreds of proteins compared to classical sucrose synaptosomes and permitted the identification of new synaptic players [7].

In the present work, we applied FASS purification of VGLUT1^{venus} excitatory synapses to PDGF-h-αS and control littermates. Label free quantitative analysis of their protein composition revealed the upregulation of 40 proteins and the down-regulation of 2 proteins. Interestingly, the multifunction translation elongation factor eEF1A1 displayed a massive drop in expression upon α-syn overexpression [1, 53]. We thus further investigated the behavior of this marker in our mouse model and *post-mortem* tissue from patients with Lewy body disease (LBD). Our results point to an early molecular event involved in α-syn mediated synapse dysfunction and loss relevant in human α-synucleinopathies.

Materials and Methods

Animals

PDGF-h-αS transgenic mice were obtained from QPS Austria Neuropharmacology (Grambach, Austria) and bred on a C57Bl/6 background [52]. The generation and characterization of the VGLUT1^{VENUS} knock-in mouse line was previously described [39]. C57Bl6 wild-type and Thy1-eGFP transgenic mice (GFP-M) were obtained from Jackson Laboratory (Bar Harbor, ME, USA). PDGF-h-αS x VGLUT1^{VENUS} (termed h-αS in this paper) and PDGF-h-αS x GFP-M lines were created by interbreeding. All animals were housed in groups under pathogen-free conditions and bred in the animal housing facility at the Center for Neuropathology and Prion Research of the Ludwig-Maximilians-University Munich, with food and water provided ad libitum (21 ± 2 °C, at 12/12-hour light/dark cycle). Breeding and experimental procedures followed the European guide for the care and use of laboratory animals and the Ethical Review Board of the Government of Upper Bavaria (Az. 55.2-1-54-2532-204-2014) and the current laws of France. All data are reported according to the ARRIVE criteria [45].

Post mortem tissue samples

Post mortem human tissue samples were obtained from the Neurobiobank Munich. All donors or their families provided written informed consent for brain donation. Samples were collected in accordance with Institutional Review Board protocols approved by the local ethics committee (#345-13). Ethics approval for the procedures of this study was granted. All procedures of this study were in accordance with the 1964 Helsinki declaration and its later amendments or comparable ethical standards. Studies were performed using tissue from patients with neuropathologically confirmed LBD [77] (n = 6) and age-matched controls (n = 5). Samples from LBD patients were at Braak stages VI [9] (Supplementary Table S4). For immunohistochemistry, formalin-fixed and paraffin-embedded tissue of the anterior cingulate gyrus was used. For Western Blot, frozen tissue of the anterior cingulate gyrus was homogenized in 10 volumes of lysis buffer (Tris-buffered saline containing 2% SDS and 1 x Complete protease inhibitor mixture (Roche)) using a OMNI TH homogenizer and centrifuged at 17000 g for 1 h at 4°C. The resulting supernatants were used for Western blotting.

Preparation of S-synaptosomes and FACS instrumentation

For the enrichment of glutamatergic synaptosomes and the concurrent study of proteomic changes due to excess α-syn, we used mice carrying the VGLUT1^{VENUS} knock-in [39] and the PDGF-h-αS transgene [52] at 12-13 weeks of age. Littermates negative for h-αS were used as controls. The S-synaptosome preparation was adapted from a protocol previously described [7, 79]. Sample size for FASS was 12 animals (6 WT, 2x3 PDGF-h-αS x VGLUT1^{VENUS}, littermates, mixed gender, 12 weeks old). Details on synaptosome preparation and FASS gating strategy were described previously [7, 50] and additionally can be found in the Supplementary Material.

Fluorescence Activated Synaptosome Sorting (FASS) and protein recovery

Fresh S-synaptosomes were diluted, kept cold and protected from light. Directly before sorting, incubation of synaptosomes with the lipophilic styryl dye FM4-64 (1µg/µl) provided bulk red labeling of membranes. Samples were analyzed and sorted at event rates of 18000 – 22000 evt/s until approximately 80 x 10^6 particles had been collected. To test the quality of sorted samples (FASS-synaptosomes), they were reanalyzed by flow cytometry with identical instrument setting. Before proteomic analysis, FASS-synaptosomes were concentrated on polycarbonate filters with a pore size of 0.1 µm using a custom-built vacuum concentrator. Proteins were recovered with 70 µl of SDS sample buffer and sample concentration was determined through SDS-PAGE and regular silver staining.

SDS-PAGE and Western blotting

The primary antibodies used in this study are listed in Table S1. SDS-PAGE using 4-20% Mini-PROTEAN® TGX Stain-Free™ gels (Bio-Rad) were carried out according to the manufacturer's recommendations, Western blotting was performed according to standard procedures. We used fluorophore coupled secondary antibodies (Li-Cor, 1:20000) and visualized signals with an Odyssey® Classic scanner and Image Studio™ software. Quantification of bands was performed in ImageJ (National Institutes of Health) and their intensity was normalized to the intensity of bands in the entire lane, using Bio-Rad's stain-free blot technology, ImageLab software (BioRad) and a ChemiDoc™ system.

Immunofluorescence

1 ml (correlating to ~10^6 particles) of diluted FASS-synaptosomes were added on top of a 12 mm diameter gelatinized cover slip and centrifuged for 34 min at 6800 g. FASS-synaptosomes

were fixed with 4% paraformaldehyde for 20 minutes, washed and stored in PBS. Primary antibody incubation was performed overnight at 4°C, followed by secondary antibody incubation 1h at room temperature. For mounting on glass coverslips, VECTASHIELD® Mounting Medium (Vector Laboratories) was used. For immunofluorescence in free-floating sections, mice were transcardially perfused with 1x phosphate-buffered saline (PBS) and 4% paraformaldehyde under deep ketamine/xylazine anesthesia. Slice preparation and staining was performed as previously described [8].

Immunohistochemistry

Formalin-fixed, paraffin-embedded tissue was sectioned (4 µm per section), deparaffinized, and rehydrated. Immunohistochemical staining was done using primary eEF1A1 antibody, ultraView DAB Detection Kit and a Ventana BenchMark ULTRA staining instrument (Roche) according to the manufacturer's specifications. The Ventana staining procedure included pretreatment with Cell Conditioner 1 (pH 6) for 56 min, followed by incubation with 1:1000 diluted eEF1A1 antibody at room temperature for 32 min and detection with UltraView DAB (Roche). Counterstaining with hematoxyline was performed prior to dehydration and mounting. For αS staining, the same protocol was adapted to use 36 min of pretreatment and 1:1000 diluted αS antibody.

Light microscopy

Confocal imaging of FASS synaptosomes was performed on an LSM 780 (Zeiss, Jena, Germany) equipped with a 63x/1.40 oil immersion objective. Laser wavelengths used for excitation and collection range of emitted signals were as follows: Alexa488 / VGLUT1 – 488nm / –585 nm; Alexa594 – 561 nm / 585-743 nm; Alexa647 – 633 nm / 638-755 nm. For imaging FASS-synaptosomes, 16-bit data stacks of 2048 x 2048 pixels were acquired from five different fields of view on the cover slip (lateral resolution 0.082 µm/pixel, axial resolution 0.3 µm/pixel). Stimulated emission depletion (STED) microscopy images were acquired on a Leica SP8-3XSTED microscope equipped with a 100x/1.40 oil immersion objective. Laser wavelengths used for excitation and depletion were as follows: Alexa488/VGLUT1 – 488nm/670nm; Alexa594/eEF1A – 594nm/670nm. Pixel size was 22nm, bit depth set to 8bits and several frames were accumulated. Immunostained free-floating mouse brain sections were imaged accordingly: 16 bit, 1024 x 1024, lateral resolution 0.044 µm/pixel, axial resolution 0.2 µm/pixel. Confocal

imaging of apical tuft dendrites in h-αS x GFP-M mice were performed as previously described [8]. DAB-stained immunohistochemical samples of human brain tissue were digitized on an Olympus BX41 microscope equipped with an Olympus SC30 digital camera using a 40× objective.

Electron microscopy

Transmission electron microscopy was performed in the somatosensory cortex of h-αS and control mice (n = 4 per group). Detailed description of sample preparation and electron microscope settings can be found in the supplementary material.

Image processing and analysis

Analysis of spine density was performed on deconvoluted (AutoQuantX3, Media Cybernetics) confocal image stacks as previously described [8]. To quantify the immunofluorescence and VGLUT1^{VENUS} signal of individual FASS-synaptosomes, custom-written MATLAB cluster analysis was applied. VGLUT1^{VENUS} positive synaptosomes were detected in 3D by applying the 80th percentile as minimal threshold. To separate contacting synaptosomes, the data was segmented morphologically by calculating the distance transformation, followed by watershed segmentation along minimal distance ridges. Only structures with a volume > 0.15 µm^3 were counted as synaptosomes. The volume of each synaptosome was refined to correct for photon scattering. For this, the half-width VGLUT1^{VENUS} intensity was calculated and was used as a minimal threshold for the final dimension. The mean and summed VGLUT1^{VENUS} fluorescence signal and the immunofluorescence signal were calculated for the center plane of each synaptosome. In the case of postsynaptic proteins, the immunofluorescence commonly appears somewhat off the synaptosome. Therefore, the mean and summed immune signal was derived from contacting immunopositive structures. All images were recorded with identical laser power and microscope settings on the same day. Due to the thin sample size of 1 µm (diameter of single synaptosome), photon aberration only marginally deteriorates the signal intensity. Thus, detected fluorescence intensity constitutes a quantitative measure of the amount of labeled protein per synaptosome. Detection and quantification of eEF1A1, VLGUT1 and PSD95 positive structures in mouse brain tissue was performed using Imaris v.7.7.2 (Bitplane Inc.) software with the spot detection algorithm (XY diameter: 0.5 µm

(PSD95) or 0.7 µm (eEF1A1 / VGLUT1); Z diameter: 1.4 µm). Background subtraction was enabled and region growing type was set to local contrast with a manual threshold of 30 defined for all datasets. Spots were filtered for volume > 0.01 μm^2. The data was compiled in MATLAB using ImarisXT interface. Color images from IHC stainings were color deconvoluted and converted to grayscale using ImageJ. Of the resulting image, the average intensity was calculated using inverted LUT, so that lower values represent weaker immunosignal. TEM micrographs were analyzed with ImageJ, to measure the presynaptic area, length of post synaptic density (PSD) and the number synaptic vesicles (SV) to calculate vesicle density. For quantification of DAB staining intensity in neurons, cell body were detected semi-automatically using CellProfiler 3.0 [14].

Proteomics

Sample preparation and nano-MS/MS as well as label-free quantitative data analysis and results processing are described in detail in the supplementary material.

Proteomics data archival

The mass spectrometry proteomics data have been deposited to the ProteomeXchange Consortium (http://proteomecentral.proteomexchange.org) via the PRIDE partner repository [76] and can be accessed by reviewers with the dataset identifier PXD006812, the username reviewer91501@ebi.ac.uk and the password **08CethU6**.

Bioinformatics

Gene ontology term and KEGG pathway analyses were done using DAVID Bioinformatics Resources 6.8, National Institute of Allergy and Infectious Diseases (NIAID), NIH [42, 43].

Statistics

The sample size of animals per experiment was chosen according to our previous experience. Sample sizes of human material were based on tissue availability. Graphs were created and statistics were calculated in Prism v 7.04 (GraphPad Software, San Diego, CA, USA). For assessment of inter-group differences at single time points, Student's *t*-test (unpaired, two-sided) was applied. Normal distribution was assumed according to the central limit theorem, as spine densities and immunofluorescence of FASS-synaptosomes were calculated as the means of means for every mouse. For *t*-tests, the variance between groups was tested (F-test) and not found

to be significantly different. For comparing cumulative distributions, Kolmogorov-Smirnov Test (KS test) was used. Data are expressed as mean ± s.e.m., with $p = 0.05$ as significance threshold (*$p < 0.05$; **$p < 0.01$; ***$p < 0.001$).

Results

Screening for proteins in VGLUT1-containing synapses by FASS

Our previous work showed that mice overexpressing human α-syn (PDGF-h-αS mice) progressively lose dendritic spines of excitatory cortical neurons [8]. Confocal imaging and analysis of apical tuft dendrites from layer V somatosensory cortical neurons in PDGF-h-αS x GFP-M mice shows that dendritic spine density is not significantly different in mice aged 8 weeks (Fig. 1A). However, at 18 weeks of age, a reduction of spine density is present h-αS mice, indicating that spine loss starts to occur in an age-dependent manner at around 12 weeks in these mice. Using this observation as a basis, we set out to investigate which changes in the protein composition of glutamatergic synapses might contribute to this phenotype.

The experimental workflow including synaptosome purification using FASS and validation using Western blot, immunofluorescence and immunohistochemistry of mouse and human brain tissue is illustrated in Fig. 1B. During the FASS procedure, $80x10^6$ FASS-synaptosomes were collected from each mouse sample for proteomic analysis. Additional 1×10^6 FASS-synaptosomes were sedimented onto glass coverslips for immunofluorescence imaging (Fig. 1B). Endogenous $VGLUT1^{VENUS}$ expression in homogenates and S-synaptosomes of the mice used for FASS was found to be not significantly different (Fig. 1C). Before sorting, S-synaptosome preparations contained ~30% $VGLUT1^{VENUS}$ fluorescent particles eligible for sorting (ctrl: 28.7 ± 2.35 %; αS: 31.6 ± 1.98 %). After FASS sorting, the fraction of $VGLUT1^{VENUS}$ positive particles increased to ~ 65% (ctrl: 65.9 ± 1.44 %; αS: 64.4 ± 0.94 %) (Fig. 1D). The enrichment in $VGLUT1^{VENUS}$ fluorescent particles was comparable across all samples (Fig. 1E).

To systematically assess differences in protein composition of synapses in αS animals versus controls, we used MS-based protein identification and label-free quantification. Samples (n = 3

mice per group) were separated by one-dimensional SDS-PAGE, tryptically digested in the gel and analyzed by nano LC-MS/MS followed by protein database search using SEQUEST as a search engine. About 1200 protein groups where identified and quantified by label-free mass spectrometry. After statistical testing using ANOVA, 115 proteins were found to be significantly changed in h-αS overexpressing mouse brains compared to controls. Considering only hits with at least two unique peptides identified left 42 differentially expressed proteins (see Supplementary Table S2). Furthermore, the overexpression of human α-syn in the h-αS mice on the protein level was confirmed by Western blots of homogenates and S-Synaptosomes (Supplementary Fig. 1A) and quantitative MS data of FASS-synaptosomes (Supplementary Fig. 1B).

Overexpression of alpha-synuclein induces an increased expression of proteins at synapses

Of the 42 differentially expressed proteins, the majority displayed an increased abundance in h-αS samples (Fig. 2A). Therefore, we tested whether this trend may result from structural alterations e.g. an increased number of synaptic vesicles per presynapse. We therefore performed transmission electron microscopy and measured the presynaptic area, the postsynaptic density length, the number and density of synaptic vesicles. We did not observe any difference between control and h-αS mice on any of these parameters (Supplementary Fig. 2).

Among the significantly upregulated targets are proteins of the endocytic machinery (Ap2a1, Ap2b1), intracellular trafficking-related Rab GTPases (Rab1b, Rab3a), regulators of ER structure and function (Rtn4, Rtn1) and Ca^{2+} homeostasis (Ppp3r1), cytoskeleton and associated proteins (Tuba4a, Tubb2a/3/4a/5, Actn1, Mapt (better known as tau)), mitochondrial proteins (Ndufv1, Ndufs6), synaptic vesicle proteins (Syngr1, Syngr3) and the synaptic vesicle exocytosis regulator Stxbp1, better known as Munc-18-1. The 42 proteins that we found to be significantly enriched or

depleted in our PDGF-h-αS x VGLUT1^{VENUS} samples were further classified according to their ascribed cellular localization and molecular function using gene ontology (GO) terms (Supplementary Fig. 3A).

To validate the proteomic analysis, we performed a series of Western blots on homogenates and conventional S-synaptosomes as well as quantitative immunofluorescence imaging on VGLUT1^{VENUS} FASS-synaptosomes targeting several protein hits. While no h-αS-related changes could be detected in homogenates, we observed a significant increase of synaptogyrin 1 and Munc18-1 in S-synaptosomes. Increased levels of ß-tubulin, synaptogyrin 3, and tau were not yet confirmed (Supplementary Fig. 3 C-E).

Besides the overexpressed proteins, the translation elongation factor eEF1A1 stands out by its strong depletion in h-αS samples down to about 8% of the mean normalized eEF1A1 abundance of controls (Supplementary Table S2). This protein has apart from its role as a translation factor several non-canonical functions in synaptic plasticity and was therefore regarded with special attention in the following study.

Bioinformatic cluster analysis indicates α-syn mediated disruption of the synaptic protein network

In order to better understand which cellular pathways are altered in response to α-syn overexpression, we performed KEGG pathway and gene ontology (GO) term analyses on the proteins which were found to be differentially expressed in h-αS mice (Fig. 2B).

KEGG pathway enrichment analysis showed those pathways significantly enriched which contribute to neurotransmitter release, such as “synaptic vesicle cycle” or “calcium reabsorption”. Furthermore, pathways related to Alzheimer’s disease and Huntington’s disease were significantly enriched (Fig. 2B). Similarly, GO classification revealed molecular functions related

to neurotransmission, such as 'GTPase activity' and 'GTP binding', which are involved in vesicle cycling via small G-proteins and presynaptic modulation of transmitter release via G-protein coupled neurotransmitter receptors (Supplementary Fig. 3A).

In order to determine the network of proteins interacting with those that were differentially expressed in tissue overexpressing α-syn, we performed an IntAct database analysis using DAVID Bioinformatics Resources 6.8 [42, 43]. This revealed, among others, a number of 14-3-3 constituents (Ywhab, Ywhaz and Ywhae), which are known for their interaction with α-syn aggregation intermediates and their presence in Lewy bodies [63]. Additional interaction partners were for example PSD95 (Dlg4) or NMDA channel subunits (Grin2b, Grin1) (Fig. 2C). While these were, as expected by the input, proteins typically involved in synaptic function, eEF1A1 was listed as an interaction partner in a majority of the results (Supplementary Table S3). These results suggest that eEF1A1 may play a critical role in the regulation of synaptic function. We therefore decided to further characterize eEF1A1 in h-αS mice and human cases of Lewy body disease.

Validation of the differential expression of eEF1A1 in synaptosomes

Quantitative MS data showed a marked reduction in the normalized abundance of eEF1A1 in PDGF-h-αS x VGLUT1^{VENUS} FASS synaptosomes, with a fold change of 0.08 compared to control. To confirm this down-regulation, Western blots were performed with the homogenates and S-synaptosomal fractions. While the eEF1A1 level in was significantly lower in S-synaptosomes of αS animals compared to wild-type littermates, it was unchanged in homogenates (Fig. 3A).

During FASS, 10^6 FASS-synaptosomes per sample were further collected and fixed on glass coverslips. Immunofluorescence confocal imaging followed by analysis of VGLUT1^{VENUS} and

eEF1A1 intensities allowed to confirm the local reduction of eEF1A1 signal at individual VGLUT1^{VENUS} FASS synaptosomes (Fig. 3B). Fig. 3C shows eEF1A1 immunosignal projections from 48 randomly selected FASS-synaptosomes, aligned for better representation. In the sample from αS overexpressing animals (Fig. 3c2), the signal is reduced, which is especially relevant for structures expressing larger amounts of eEF1A1. The cumulative frequency distribution of the relative eEF1A1/VGLUT1^{VENUS} fluorescence shows a shift to the left in αS samples compared to controls, confirming lower eEF1A1 signal in these synaptosomes (Fig. 3D). A reduction of the integrated eEF1A1 immunofluorescence in relation to VGLUT1^{VENUS} signal intensity can also be observed in a representation of all imaged FASS synaptosomes (n = 630-755 measurements per sample) (Fig. 3E). Consequently, the mean relative eEF1A1 intensity is significantly lower in FASS VGLUT1^{VENUS} synaptosomes derived from αS animals (Fig. 3F).

As synaptosomes consist mainly of the resealed presynaptic element associated to the unsealed tip of the postsynaptic spine [7, 37], we further determined eEF1A1 protein subcellular localization using stimulated-emission-depletion microscopy (STED) with a resolution of 60 nm. In most synaptosomes, eEF1A1 immunofluorescence colocalized with VGLUT1^{VENUS} signal while additional dots were opposed to pre-synapses (Fig. 3G). We therefore conclude that the eEF1A1 protein is present on both sides of synapses and may be directly impacted by presynaptic pathological processes induced by α-syn.

eEF1A1 is reduced in the brain tissue of h-αS mice

As we were interested in the expression and distribution of eEF1A1 in intact tissue, we next examined eEF1A1 protein levels in brain tissue of 12-week-old PDGF-h-αS x VGLUT1^{VENUS} mice. Two brain regions were investigated using immunofluorescence staining against eEF1A1 and confocal microscopy: layer I of the cingulate cortex and the somatosensory cortex. (Fig. 4A),

in which data on spine loss had been acquired previously. The fluorescence intensity of eEF1A1 positive puncta as well as their number was analyzed (Fig. 4B). We found a strong reduction in eEF1A1 staining intensity in both the cingulate and the somatosensory cortex (Fig. 4C, Supplementary Fig. 4A). As in one of the brain areas a small but significant difference in endogenous VGLUT1^{VENUS} expression was measured (Supplementary Fig. 4B), we used the mean eEF1A1/VGLUT1^{VENUS} fluorescence intensity for statistical comparison. The ratio proved to be profoundly reduced in h-αS tissue (Fig. 4D). Additionally, a reduction of the density of eEF1A1 positive puncta was detected in the two cortical areas of h-αS mice (Fig. 4E), whereas the mean puncta volume was unchanged between groups (Supplementary Fig. 4C).

Similarly, we approached the question whether a change in the amount of excitatory postsynapses is present in this mouse brain tissue. Correlating with the loss of eEF1A1 in h-αS mouse samples, we indeed observed reduced PSD95 immunofluorescence intensity in these brains (Fig. 4F, G), accompanied by a loss of PSD95 positive structures in the tissue (Fig. 4H). In this way, we confirm that spine loss is present at 12 weeks in h-αS mice and at the time of experimental procedures in this study.

eEF1A1 is reduced in the neuropil of human LBD cases

In order to translate our findings to human cases, we investigated the expression of eEF1A1 in the cingulate gyrus of LBD brains compared to age-matched controls. In cortical homogenates (cingulate cortex) we didn't observe a significant difference in eEF1A1 levels between control and LBD brains (Fig 5A, B). Noticeably, PSD95 expression was reduced in LBD brains (Fig. 5A, C), indicating a loss of cortical synapses. We therefore applied IHC to assess potential changes of eEF1A1 expression in the neuropil. We included tissue from mid-stage (classified as Braak stages 3 or 4) and late-stage (Braak stages 5 or 6) LBD patients. Late-stage LDB cases featured

significant cortical Lewy pathology (Fig. 5D and Supplementary Fig 5A). We performed eEF1A1 immunohistochemistry on formalin-fixed, paraffin-embedded tissue sections from the human cingulate gyrus. LBD cases from both mid- and late-stage groups showed less intense DAB staining patterns compared to controls (Fig. 5E, Supplementary Fig. 5B). Strikingly, quantification of the eEF1A1 signal revealed significantly reduced values in the neuropil of LBD brains, whereas the DAB staining intensity within cell bodies was comparable between groups (Fig. 5F, Supplementary Fig. 5C). Existing co-pathologies had no effect on this observation (Supplementary Fig. 6). This indicates that α-syn mediated reduction in eEF1A1 is not only present in the tissue of our mouse model, but also in human cases of LBD and that in both cases, this reduction is mainly at the level of synapses.

Discussion

Synapses are vulnerable to misfolded protein species like α-syn and their degeneration is crucially involved in the pathogenesis of neurodegenerative diseases [12]. Moreover, dendritic spine loss has been described as a structural correlate for cognitive impairment and dementia [4, 25, 62, 73]. As we have observed early spine loss in the cerebral cortex of mice overexpressing α-syn [8] which precedes the onset of motor impairments by several months [2, 52], we aimed to elucidate changes on the protein level in excitatory synapses that might explain the early synaptopathy induced by α-syn overexpression. We used fluorescence activated synaptosome sorting of VGLUT1^{VENUS} expressing synapses to achieve a 2- to 3-fold enrichment of glutamatergic synaptosomes compared to conventional preparations. Proteomic analysis of our FASS samples yielded 42 proteins differentially expressed in samples overexpressing human α-syn, most of which were upregulated compared to controls.

Although FASS provides limited amounts of synaptosome material for analysis, the removal of extra-synaptic compartments allowed us to obtain valuable and valid results with regards to existing literature on α-syn function and pathogenicity at glutamatergic synapses. The fact that the differential expression of identified proteins was not detected on our homogenates and - in most cases - S-synaptosomes indicates that local defects at glutamatergic synapses rather than global defects at the neuron level are present at the onset of disease progression. Our experiments suggest α-syn related changes in vesicle trafficking, cytoskeleton, ER- and Ca^{2+} homeostasis and mitochondrial metabolism.

Synucleins are known to be involved in the trafficking of synaptic vesicles [24, 31, 48, 59, 67, 81]. We identified upregulation of several proteins important for the synaptic vesicle cycle (Syngr1, Syngr3, Rab3A, Munc18-1, Nsf, Ap2a1, Ap2b1, Ap2m1, Sh3glb2). Previous studies in

LBD and α-syn mouse models have shown an abnormal interaction between α-syn and Rab3A, Rab5 and Rab8, thereby disrupting endocytic and secretory pathways [75, 78]. In our proteomic screen, we also found the synaptic vesicle proteins Syngr1 and Munc18-1 elevated in h-αS mice, which was confirmed by Western blot of S-synaptosomes, but not of homogenates. Apart from its role in regulation of exocytosis, Munc18-1 has been shown to serve as a chaperone controlling α-syn aggregation [16] and its upregulation might counteract both directly the aggregation propensity of α-syn by stabilizing the aggregation-resistant membrane-bound forms of α-syn and indirectly a decrease in functional Munc18-1 for secretion of synaptic vesicles due to co-aggregation with α-syn.

Similarly, α-syn directly interacts with members of the cytoskeleton like βIII-tubulin and the microtubule-associated protein tau (Mapt) [15]. Native α-syn also acts as a microtubule associated protein, facilitating microtubule polymerization and neurite outgrowth in cultured neurons [47]. In the pathologic condition, its interaction with tubulin and tau facilitates intracellular α-syn accumulation, impairing microtubule stability and microtubule-mediated transport [58, 64, 71]. A recent study reveals synaptogyrin-3 as specific interactor of mislocalized, presynaptic tau, restricting synaptic vesicle mobility and driving defects in neurotransmission in fly and mouse models of tauopathy [55]. Both Syngr3 and tau were found to be elevated in our proteomic data from h-αS mice, along with several tubulin subunits (Tuba4a, Tubb2a/3/4a/5). Though validation analysis revealed a trend towards an increase for Syngr3 and Tau in S-synaptosomes and for Syngr3, tau and β-tubulin in FASS-synaptosomes without reaching significance, further investigations will be required to confirm the upregulation of those targets. Our results provide evidence for disease-related alterations of cytoskeletal and synaptic vesicle dynamics and open perspectives for future research.

A further line of evidence in our proteomic study implies the involvement of organelles and proteins regulating cytosolic Ca^{2+} homeostasis, which are found elevated in our h-αS FASS-synaptosomes (Ppp3r1, Rtn4, Rtn1, Ndufs6, Ndufv1). Indeed, previous work identified that increasing levels of α-syn proportionally increase cytoplasmic Ca^{2+} concentrations and drive cascade engaging Calcineurin (Ppp3r1) and substrates that result in toxicity in mammalian cells [13]. Similarly, the reticulon proteins (Rtn4, Rtn1) are regulators of ER structure and Ca^{2+} homeostasis and have a pro-apoptotic function mediated by the induction of ER stress [23]. Several proteins of our screen further point towards alterations in mitochondrial energy metabolism, which is in line with previous studies on Parkinson's disease [41]. Wild-type α-syn is present in mitochondria-associated ER membranes (MAM), regulating the mitochondrial calcium homeostasis [11, 36]. Finally α-syn has also been shown to directly induce changes in mitochondria fission [57].

The translation factor eEF1A1 stands out by its strong depletion in our h-αS FASS-synaptosomes. We validated our finding in S-synaptosomes as well as in FASS-synaptosomes originating from the same mice as the proteomic data. The translation capacity of eEF1A1 and its potential to regulate actin dynamics and spine size predestine it for the control of synaptic plasticity at the protein level. Together with other proteins locally translated at synapses, a functional synergy in order to maintain long-term potentiation (LTP) by signaling through the mTOR pathway is established [74]. Additionally, the expression of eEF1A1 at nerve terminals has been shown to be essential for maintaining newly grown synapses [33].

Both pre- and postsynaptic compartments have previously been demonstrated to express eEF1A1, which is well in line with our observations. Using STED microscopy, we found the eEF1A1 immunosignal both colocalized with and excluded from $VGLUT1^{VENUS}$ fluorescence in

single excitatory synaptosomes. On the presynaptic side, eEF1A1 transcripts are enriched in mature CNS axons and are reduced following axonal injury [72]. An increasing literature support the notion that the protein synthesis machinery is active within CNS axons and involved in synaptic plasticity [69]. Furthermore, several translation factor mRNAs including eEF1a1 mRNA have been reported at the local transcriptome of presynapses [37]. eEFs also link up with the p70S6K pathway to protein expression in neurites and synapses, where they promote NGF-induced neurite outgrowth [38, 44, 61], synapse formation and stabilization. Likewise, eEF1A1 has been convincingly shown to be associated with dendrites and excitatory postsynapses and more specifically, the postsynaptic density within dendritic spines via binding actin [17, 18, 28] and it was shown that eEF1A1 knockdown significantly decreases PSD95 expression levels *in vitro* [30]. Here, we extend this knowledge to the mouse brain, showing that a reduction of eEF1A1 is concomitant with a reduction in PSD95 intensity and spot density. It connects our previous finding of dendritic spine loss to eEF1A1's other, non-canonical functions. eEF1A1 regulates cytoskeletal dynamics by bundling F-actin and binding to microtubules [10, 35, 46, 82], acts protective against apoptosis [65] and regulates M4 muscarinic acetylcholine receptor recycling [54] and protein degradation [19]. Furthermore, a recent study demonstrated that a CTIF-eEF1A1-DCTN complex links selective recognition and aggresomal targeting of misfolded α-syn. This process is accompanied by a sequestration of CTIF and possibly eEF1A1 into the aggresome, which might in turn decrease the amount of synaptic eEF1A1 [60]. Additionally, α-syn toxicity and the corresponding elevation of synaptic Ca^{2+} could disrupt eEF1A1 dimer formation and lead to decreased F-actin bundling impairing spine stabilization [10].

Strikingly, human brain tissue from LBD patients also showed reduced eEF1A1 staining intensity in the densely synaptic layer I of the cingulate cortex. We observed this in advanced stages of the disease (Braak 5/6) as well as earlier stages (Braak 3/4) in which no or very mild αS

pathology is present in the neocortex. At the same time, differences in eEF1A1 expression were not detectable in cortex homogenates of late-stage LBD, whereas a reduction of overall PSD95 expression was present. Together, these results indicate a local, pathophysiological role for eEF1A1 at synapses early in LBD. As *de novo* protein synthesis and cytoskeleton remodeling links chemically or electrically induced changes in synaptic strength to structural adaptations, it is the basis for memory consolidation in the brain and depletion of eEF1A1 can contribute to structural impairments observed in neurodegenerative conditions. In fact, a study in Alzheimer's disease brains has connected dysregulated eEF1A expression to synaptic plasticity impairments [3] and defects in *de novo* protein synthesis have been demonstrated in several neurodegenerative disorders characterized by impaired synaptic plasticity, including Parkinson's disease, Alzheimer's disease, frontotemporal lobar degeneration and prion diseases [22, 32, 51, 56]. We therefore propose that eEF1A1 could serve as an early and universal marker for neurodegenerative diseases characterized by synapse loss.

Our study highlights for the first time the functional role of eEF1A1 in α-synucleinopathies and opens new perspectives about the involvement of eEF1A1 in α-synucleinopathies. We therefore propose a model, in which synaptic eEF1A1 reduction is an early and central event, which is caused by a disruption of α-syn balance and may mediate alterations in the organization of the cytoskeleton, phagosomal activity and ultimately leads to synaptopathy. By altering the normal half-life of eEF1A1, estimated to be 4.7 days [20], α-syn overexpression might furthermore indirectly affect the turn-over of other presynaptic proteins and approaching this question could be subject to future research. A more detailed understanding of the role of eEF1A proteins in the pathogenesis of α-synucleinopathies still remains to be determined. It will be important to investigate the mechanistic link between synaptic translation and α-syn mediated

synaptopathy in the future and to determine whether eEF1A1 or its upstream factors like the eukaryotic initiation factor 2α (eIF2α) represent genuine targets for novel therapeutic approaches.

Acknowledgements:

We thank Sarah Hanselka, Katharina Bayer, Michael Schmidt, Dr. Christelle Martin, Melissa Deshors, Dr. Norbert Buresch (Neurobiobank Munich), Dr. Vincent Pitard (Flow cytometry facility, CNRS UMS 3427, INSERM US 005, Univ. Bordeaux), Patrice Mascalchi (Bordeaux Imaging Center, CNRS, INSERM, Univ. Bordeaux) and the Biochemistry & biophysics facility of Bordeaux Neurocampus (CNRS, INSERM, Univ. Bordeaux) for their excellent technical support and animal care. We are also thankful towards Stephan Müller for his expertise in proteomics and advice on our data.

Funding:

This work was funded by the Munich Cluster for Systems Neurology SyNergy (EXC1010) to SB, SC and JH; the German Academic Exchange Service (DAAD) to SB; the French Agence Nationale de la Recherche (ANR-12-JSV4-0005-01 VGLUT-IQ and ANR-10-LABX-43 BRAIN) to EH; the Fondation pour la Recherche Médicale (ING20150532192) to EH and the CNRS PICS program to EH.

Conflict of interest:

The authors declare that they have no conflict of interest.

Author contribution:

SB performed design of the experiment, subcellular fractioning, FASS sorting, validation of results in mouse and human tissue, bioinformatics and interpretation of results and wrote the manuscript. MFA provided expertise and performed subcellular fractioning, FASS sorting and Western blotting with SB. FP performed programming for image analysis. MMD performed bioinformatic analyses. MMD, VR and TA selected human tissue and provided neuropathological expertise. ML performed EM experiments and EM data analysis. SCl performed mass spectrometry and analysis of the MS raw data. SCr and LS provided technical support. MMD, MFA, ML, SCr and SCl helped with manuscript preparation. EH performed STED microscopy. EH and JH supervised the study, contributed to conception, design and manuscript writing and provided financial support and final approval of the manuscript.

Ethical approval: All procedures performed in studies involving human participants were in accordance with the ethical standards of the institutional and/or national research committee and with the 1964 Helsinki declaration and its later amendments or comparable ethical standards. All

applicable international, national, and/or institutional guidelines for the care and use of animals were followed.

References

1. Abbas W, Kumar A, Herbein G (2015) The eEF1A Proteins: At the Crossroads of Oncogenesis, Apoptosis, and Viral Infections. Front Oncol 5:75. doi: 10.3389/fonc.2015.00075

2. Amschl D, Neddens J, Havas D, Flunkert S, Rabl R, Römer H, Rockenstein E, Masliah E, Windisch M, Hutter-Paier B (2013) Time course and progression of wild type α-Synuclein accumulation in a transgenic mouse model. BMC Neurosci 14:1

3. Beckelman BC, Day S, Zhou X, Donohue M, Gouras GK, Klann E, Keene CD, Ma T (2016) Dysregulation of Elongation Factor 1A Expression is Correlated with Synaptic Plasticity Impairments in Alzheimer's Disease. J Alzheimers Dis JAD 54:669–678. doi: 10.3233/JAD-160036

4. Bellucci A, Zaltieri M, Navarria L, Grigoletto J, Missale C, Spano P (2012) From α-synuclein to synaptic dysfunctions: new insights into the pathophysiology of Parkinson's disease. Brain Res 1476:183–202. doi: 10.1016/j.brainres.2012.04.014

5. Ben Gedalya T, Loeb V, Israeli E, Altschuler Y, Selkoe DJ, Sharon R (2009) α-Synuclein and Polyunsaturated Fatty Acids Promote Clathrin-Mediated Endocytosis and Synaptic Vesicle Recycling. Traffic 10:218–234. doi: 10.1111/j.1600-0854.2008.00853.x

6. Bendor JT, Logan TP, Edwards RH (2013) The Function of α-Synuclein. Neuron 79:1044–1066. doi: 10.1016/j.neuron.2013.09.004

7. Biesemann C, Grønborg M, Luquet E, Wichert SP, Bernard V, Bungers SR, Cooper B, Varoqueaux F, Li L, Byrne JA, Urlaub H, Jahn O, Brose N, Herzog E (2014) Proteomic screening of glutamatergic mouse brain synaptosomes isolated by fluorescence activated sorting. EMBO J 33:157–170. doi: 10.1002/embj.201386120

8. Blumenstock S, Rodrigues EF, Peters F, Blazquez-Llorca L, Schmidt F, Giese A, Herms J (2017) Seeding and transgenic overexpression of alpha-synuclein triggers dendritic spine pathology in the neocortex. EMBO Mol Med 9:716–731. doi: 10.15252/emmm.201607305

9. Braak H, Del Tredici K, Rüb U, de Vos RA, Steur ENJ, Braak E (2003) Staging of brain pathology related to sporadic Parkinson's disease. Neurobiol Aging 24:197–211

10. Bunai F, Ando K, Ueno H, Numata O (2006) Tetrahymena Eukaryotic Translation Elongation Factor 1A (eEF1A) Bundles Filamentous Actin through Dimer Formation. J Biochem (Tokyo) 140:393–399. doi: 10.1093/jb/mvj169

11. Calì T, Ottolini D, Negro A, Brini M (2012) α-Synuclein Controls Mitochondrial Calcium Homeostasis by Enhancing Endoplasmic Reticulum-Mitochondria Interactions. J Biol Chem 287:17914–17929. doi: 10.1074/jbc.M111.302794

12. Calo L, Wegrzynowicz M, Santivañez-Perez J, Grazia Spillantini M (2016) Synaptic failure and α-synuclein. Mov Disord 31:169–177. doi: 10.1002/mds.26479

13. Caraveo G, Auluck PK, Whitesell L, Chung CY, Baru V, Mosharov EV, Yan X, Ben-Johny M, Soste M, Picotti P, Kim H, Caldwell KA, Caldwell GA, Sulzer D, Yue DT, Lindquist S (2014) Calcineurin

determines toxic versus beneficial responses to -synuclein. Proc Natl Acad Sci 111:E3544–E3552. doi: 10.1073/pnas.1413201111

14. Carpenter AE, Jones TR, Lamprecht MR, Clarke C, Kang IH, Friman O, Guertin DA, Chang JH, Lindquist RA, Moffat J, Golland P, Sabatini DM (2006) CellProfiler: image analysis software for identifying and quantifying cell phenotypes. Genome Biol 7:R100. doi: 10.1186/gb-2006-7-10-r100

15. Cartelli D, Aliverti A, Barbiroli A, Santambrogio C, Ragg EM, Casagrande FVM, Cantele F, Beltramone S, Marangon J, De Gregorio C, Pandini V, Emanuele M, Chieregatti E, Pieraccini S, Holmqvist S, Bubacco L, Roybon L, Pezzoli G, Grandori R, Arnal I, Cappelletti G (2016) α-Synuclein is a Novel Microtubule Dynamase. Sci Rep 6:33289. doi: 10.1038/srep33289

16. Chai YJ, Sierecki E, Tomatis VM, Gormal RS, Giles N, Morrow IC, Xia D, Götz J, Parton RG, Collins BM, Gambin Y, Meunier FA (2016) Munc18-1 is a molecular chaperone for α-synuclein, controlling its self-replicating aggregation. J Cell Biol 214:705–718. doi: 10.1083/jcb.201512016

17. Cho S-J, Jung J-S, Ko BH, Jin I, Moon IS (2004) Presence of translation elongation factor-1A (eEF1A) in the excitatory postsynaptic density of rat cerebral cortex. Neurosci Lett 366:29–33. doi: 10.1016/j.neulet.2004.05.036

18. Cho S-J, Lee H-S, Dutta S, Seog D-H, Moon I-S (2012) Translation elongation factor-1A1 (eEF1A1) localizes to the spine by domain III. BMB Rep 45:227–232. doi: 10.5483/BMBRep.2012.45.4.227

19. Chuang S-M, Chen L, Lambertson D, Anand M, Kinzy TG, Madura K (2005) Proteasome-Mediated Degradation of Cotranslationally Damaged Proteins Involves Translation Elongation Factor 1A. Mol Cell Biol 25:403–413. doi: 10.1128/MCB.25.1.403-413.2005

20. Cohen LD, Zuchman R, Sorokina O, Müller A, Dieterich DC, Armstrong JD, Ziv T, Ziv NE (2013) Metabolic turnover of synaptic proteins: kinetics, interdependencies and implications for synaptic maintenance. PloS One 8:e63191. doi: 10.1371/journal.pone.0063191

21. De Robertis E, Rodriguez De Lores Arnaiz G, Pellegrino De Iraldi A (1962) Isolation of synaptic vesicles from nerve endings of the rat brain. Nature 194:794–795

22. Delaidelli A, Jan A, Herms J, Sorensen PH (2019) Translational control in brain pathologies: biological significance and therapeutic opportunities. Acta Neuropathol (Berl) 137:535–555. doi: 10.1007/s00401-019-01971-8

23. Di Sano F, Piacentini M (2012) Reticulon Protein-1C: A New Hope in the Treatment of Different Neuronal Diseases. Int J Cell Biol 2012:1–9. doi: 10.1155/2012/651805

24. Diao J, Burré J, Vivona S, Cipriano DJ, Sharma M, Kyoung M, Südhof TC, Brunger AT (2013) Native α-synuclein induces clustering of synaptic-vesicle mimics via binding to phospholipids and synaptobrevin-2/VAMP2. eLife 2. doi: 10.7554/eLife.00592

25. Dickson DW, Crystal HA, Bevona C, Honer W, Vincent I, Davies P (1995) Correlations of synaptic and pathological markers with cognition of the elderly. Neurobiol Aging 16:285–298. doi: 10.1016/0197-4580(95)00013-5

26. Dieterich DC, Kreutz MR (2016) Proteomics of the Synapse--A Quantitative Approach to Neuronal Plasticity. Mol Cell Proteomics MCP 15:368–381. doi: 10.1074/mcp.R115.051482

27. Emanuele M, Esposito A, Camerini S, Antonucci F, Ferrara S, Seghezza S, Catelani T, Crescenzi M, Marotta R, Canale C, Matteoli M, Menna E, Chieregatti E (2016) Exogenous Alpha-Synuclein Alters Pre- and Post-Synaptic Activity by Fragmenting Lipid Rafts. EBioMedicine 7:191–204. doi: 10.1016/j.ebiom.2016.03.038

28. Fernández E, Collins MO, Uren RT, Kopanitsa MV, Komiyama NH, Croning MDR, Zografos L, Armstrong JD, Choudhary JS, Grant SGN (2009) Targeted tandem affinity purification of PSD-95 recovers core postsynaptic complexes and schizophrenia susceptibility proteins. Mol Syst Biol 5:269. doi: 10.1038/msb.2009.27

29. Fortin DL (2004) Lipid Rafts Mediate the Synaptic Localization of α-Synuclein. J Neurosci 24:6715–6723. doi: 10.1523/JNEUROSCI.1594-04.2004

30. Fujimura M, Usuki F, Cheng J, Zhao W (2016) Prenatal low-dose methylmercury exposure impairs neurite outgrowth and synaptic protein expression and suppresses TrkA pathway activity and eEF1A1 expression in the rat cerebellum. Toxicol Appl Pharmacol 298:1–8. doi: 10.1016/j.taap.2016.03.002

31. Fusco G, Pape T, Stephens AD, Mahou P, Costa AR, Kaminski CF, Kaminski Schierle GS, Vendruscolo M, Veglia G, Dobson CM, De Simone A (2016) Structural basis of synaptic vesicle assembly promoted by α-synuclein. Nat Commun 7:12563. doi: 10.1038/ncomms12563

32. Garcia-Esparcia P, Hernández-Ortega K, Koneti A, Gil L, Delgado-Morales R, Castaño E, Carmona M, Ferrer I (2015) Altered machinery of protein synthesis is region- and stage-dependent and is associated with α-synuclein oligomers in Parkinson's disease. Acta Neuropathol Commun 3:76. doi: 10.1186/s40478-015-0257-4

33. Giustetto M, Hegde AN, Si K, Casadio A, Inokuchi K, Pei W, Kandel ER, Schwartz JH (2003) Axonal transport of eukaryotic translation elongation factor 1α mRNA couples transcription in the nucleus to long-term facilitation at the synapse. Proc Natl Acad Sci 100:13680–13685

34. Gray EG, Whittaker VP (1962) The isolation of nerve endings from brain: an electron-microscopic study of cell fragments derived by homogenization and centrifugation. J Anat 96:79–88

35. Gross SR, Kinzy TG (2005) Translation elongation factor 1A is essential for regulation of the actin cytoskeleton and cell morphology. Nat Struct Mol Biol 12:772–778. doi: 10.1038/nsmb979

36. Guardia-Laguarta C, Area-Gomez E, Rub C, Liu Y, Magrane J, Becker D, Voos W, Schon EA, Przedborski S (2014) α-Synuclein Is Localized to Mitochondria-Associated ER Membranes. J Neurosci 34:249–259. doi: 10.1523/JNEUROSCI.2507-13.2014

37. Hafner A-S, Donlin-Asp PG, Leitch B, Herzog E, Schuman EM (2019) Local protein synthesis is a ubiquitous feature of neuronal pre- and postsynaptic compartments. Science 364. doi: 10.1126/science.aau3644

38. Hashimoto K, Ishima T (2011) Neurite Outgrowth Mediated by Translation Elongation Factor eEF1A1: A Target for Antiplatelet Agent Cilostazol. PLoS ONE 6:e17431. doi: 10.1371/journal.pone.0017431

39. Herzog E, Nadrigny F, Silm K, Biesemann C, Helling I, Bersot T, Steffens H, Schwartzmann R, Nagerl UV, El Mestikawy S, Rhee J, Kirchhoff F, Brose N (2011) In Vivo Imaging of Intersynaptic Vesicle Exchange Using VGLUT1Venus Knock-In Mice. J Neurosci 31:15544–15559. doi: 10.1523/JNEUROSCI.2073-11.2011

40. Hosp F, Mann M (2017) A Primer on Concepts and Applications of Proteomics in Neuroscience. Neuron 96:558–571. doi: 10.1016/j.neuron.2017.09.025

41. Hu Q, Wang G (2016) Mitochondrial dysfunction in Parkinson's disease. Transl Neurodegener 5:14. doi: 10.1186/s40035-016-0060-6

42. Huang DW, Sherman BT, Lempicki RA (2008) Systematic and integrative analysis of large gene lists using DAVID bioinformatics resources. Nat Protoc 4:44–57. doi: 10.1038/nprot.2008.211

43. Huang DW, Sherman BT, Lempicki RA (2009) Bioinformatics enrichment tools: paths toward the comprehensive functional analysis of large gene lists. Nucleic Acids Res 37:1–13. doi: 10.1093/nar/gkn923

44. Iketani M, Iizuka A, Sengoku K, Kurihara Y, Nakamura F, Sasaki Y, Sato Y, Yamane M, Matsushita M, Nairn AC, Takamatsu K, Goshima Y, Takei K (2013) Regulation of neurite outgrowth mediated by localized phosphorylation of protein translational factor eEF2 in growth cones. Dev Neurobiol 73:230–246. doi: 10.1002/dneu.22058

45. Kilkenny C, Browne WJ, Cuthill IC, Emerson M, Altman DG (2012) Improving bioscience research reporting: the ARRIVE guidelines for reporting animal research. Osteoarthritis Cartilage 20:256–260

46. Liu G, Tang J, Edmonds BT, Murray J, Levin S, Condeelis J (1996) F-actin sequesters elongation factor 1alpha from interaction with aminoacyl-tRNA in a pH-dependent reaction. J Cell Biol 135:953–963

47. Liu G, Wang P, Li X, Li Y, Xu S, Uéda K, Chan P, Yu S (2013) Alpha-synuclein promotes early neurite outgrowth in cultured primary neurons. J Neural Transm 120:1331–1343. doi: 10.1007/s00702-013-0999-8

48. Logan T, Bendor J, Toupin C, Thorn K, Edwards RH (2017) α-Synuclein promotes dilation of the exocytotic fusion pore. Nat Neurosci 20:681–689. doi: 10.1038/nn.4529

49. Lotharius J, Brundin P (2002) Pathogenesis of Parkinson's disease: dopamine, vesicles and alpha-synuclein. Nat Rev Neurosci 3:932–942. doi: 10.1038/nrn983

50. Luquet E, Biesemann C, Munier A, Herzog E (2017) Purification of Synaptosome Populations Using Fluorescence-Activated Synaptosome Sorting. Methods Mol Biol Clifton NJ 1538:121–134. doi: 10.1007/978-1-4939-6688-2_10

51. Ma T, Trinh MA, Wexler AJ, Bourbon C, Gatti E, Pierre P, Cavener DR, Klann E (2013) Suppression of eIF2α kinases alleviates Alzheimer's disease–related plasticity and memory deficits. Nat Neurosci 16:1299–1305. doi: 10.1038/nn.3486

52. Masliah E (2000) Dopaminergic Loss and Inclusion Body Formation in α-Synuclein Mice: Implications for Neurodegenerative Disorders. Science 287:1265–1269. doi: 10.1126/science.287.5456.1265

53. Mateyak MK, Kinzy TG (2010) eEF1A: Thinking Outside the Ribosome. J Biol Chem 285:21209–21213. doi: 10.1074/jbc.R110.113795

54. McClatchy DB, Fang G, Levey AI (2006) Elongation Factor 1A Family Regulates the Recycling of the M4 Muscarinic Acetylcholine Receptor. Neurochem Res 31:975–988. doi: 10.1007/s11064-006-9103-1

55. McInnes J, Wierda K, Snellinx A, Bounti L, Wang Y-C, Stancu I-C, Apóstolo N, Gevaert K, Dewachter I, Spires-Jones TL, De Strooper B, De Wit J, Zhou L, Verstreken P (2018) Synaptogyrin-3 Mediates Presynaptic Dysfunction Induced by Tau. Neuron 97:823-835.e8. doi: 10.1016/j.neuron.2018.01.022

56. Moreno JA, Radford H, Peretti D, Steinert JR, Verity N, Martin MG, Halliday M, Morgan J, Dinsdale D, Ortori CA, Barrett DA, Tsaytler P, Bertolotti A, Willis AE, Bushell M, Mallucci GR (2012) Sustained translational repression by eIF2α-P mediates prion neurodegeneration. Nature 485:507–511. doi: 10.1038/nature11058

57. Nakamura K, Nemani VM, Azarbal F, Skibinski G, Levy JM, Egami K, Munishkina L, Zhang J, Gardner B, Wakabayashi J, Sesaki H, Cheng Y, Finkbeiner S, Nussbaum RL, Masliah E, Edwards RH (2011) Direct membrane association drives mitochondrial fission by the Parkinson disease-associated protein alpha-synuclein. J Biol Chem 286:20710–20726. doi: 10.1074/jbc.M110.213538

58. Nakayama K, Suzuki Y, Yazawa I (2012) Binding of neuronal α-synuclein to β-III tubulin and accumulation in a model of multiple system atrophy. Biochem Biophys Res Commun 417:1170–1175. doi: 10.1016/j.bbrc.2011.12.092

59. Nemani VM, Lu W, Berge V, Nakamura K, Onoa B, Lee MK, Chaudhry FA, Nicoll RA, Edwards RH (2010) Increased Expression of α-Synuclein Reduces Neurotransmitter Release by Inhibiting Synaptic Vesicle Reclustering after Endocytosis. Neuron 65:66–79. doi: 10.1016/j.neuron.2009.12.023

60. Park J, Park Y, Ryu I, Choi M-H, Lee HJ, Oh N, Kim K, Kim KM, Choe J, Lee C, Baik J-H, Kim YK (2017) Misfolded polypeptides are selectively recognized and transported toward aggresomes by a CED complex. Nat Commun 8:15730. doi: 10.1038/ncomms15730

61. Petroulakis E, Wang E (2002) Nerve Growth Factor Specifically Stimulates Translation of Eukaryotic Elongation Factor 1A-1 (eEF1A-1) mRNA by Recruitment to Polyribosomes in PC12 Cells. J Biol Chem 277:18718–18727. doi: 10.1074/jbc.M111782200

62. Picconi B, Piccoli G, Calabresi P (2012) Synaptic dysfunction in Parkinson's disease. Adv Exp Med Biol 970:553–572. doi: 10.1007/978-3-7091-0932-8_24

63. Plotegher N, Kumar D, Tessari I, Brucale M, Munari F, Tosatto L, Belluzzi E, Greggio E, Bisaglia M, Capaldi S, Aioanei D, Mammi S, Monaco HL, Samo B, Bubacco L (2014) The chaperone-like protein 14-3-3η interacts with human α-synuclein aggregation intermediates rerouting the amyloidogenic pathway and reducing α-synuclein cellular toxicity. Hum Mol Genet 23:5615–5629. doi: 10.1093/hmg/ddu275

64. Prots I, Veber V, Brey S, Campioni S, Buder K, Riek R, Bohm KJ, Winner B (2013) -Synuclein Oligomers Impair Neuronal Microtubule-Kinesin Interplay. J Biol Chem 288:21742–21754. doi: 10.1074/jbc.M113.451815

65. Ruest L-B, Marcotte R, Wang E (2002) Peptide Elongation Factor eEF1A-2/S1 Expression in Cultured Differentiated Myotubes and Its Protective Effect against Caspase- 3-mediated Apoptosis. J Biol Chem 277:5418–5425. doi: 10.1074/jbc.M110685200

66. Schreiner D, Savas JN, Herzog E, Brose N, de Wit J (2017) Synapse biology in the 'circuit-age'-paths toward molecular connectomics. Curr Opin Neurobiol 42:102–110. doi: 10.1016/j.conb.2016.12.004

67. Scott D, Roy S (2012) α-Synuclein inhibits intersynaptic vesicle mobility and maintains recycling-pool homeostasis. J Neurosci Off J Soc Neurosci 32:10129–10135. doi: 10.1523/JNEUROSCI.0535-12.2012

68. Sharma K, Schmitt S, Bergner CG, Tyanova S, Kannaiyan N, Manrique-Hoyos N, Kongi K, Cantuti L, Hanisch U-K, Philips M-A, Rossner MJ, Mann M, Simons M (2015) Cell type- and brain region-resolved mouse brain proteome. Nat Neurosci 18:1819–1831. doi: 10.1038/nn.4160

69. Shigeoka T, Jung H, Jung J, Turner-Bridger B, Ohk J, Lin JQ, Amieux PS, Holt CE (2016) Dynamic Axonal Translation in Developing and Mature Visual Circuits. Cell 166:181–192. doi: 10.1016/j.cell.2016.05.029

70. Spillantini MG, Schmidt ML, Lee VM, Trojanowski JQ, Jakes R, Goedert M (1997) Alpha-synuclein in Lewy bodies. Nature 388:839–840. doi: 10.1038/42166

71. Suzuki Y, Jin C, Iwase T, Yazawa I (2014) -III Tubulin Fragments Inhibit -Synuclein Accumulation in Models of Multiple System Atrophy. J Biol Chem 289:24374–24382. doi: 10.1074/jbc.M114.557215

72. Taylor AM, Berchtold NC, Perreau VM, Tu CH, Li Jeon N, Cotman CW (2009) Axonal mRNA in Uninjured and Regenerating Cortical Mammalian Axons. J Neurosci 29:4697–4707. doi: 10.1523/JNEUROSCI.6130-08.2009

73. Terry RD, Masliah E, Salmon DP, Butters N, DeTeresa R, Hill R, Hansen LA, Katzman R (1991) Physical basis of cognitive alterations in alzheimer's disease: Synapse loss is the major correlate of cognitive impairment. Ann Neurol 30:572–580. doi: 10.1002/ana.410300410

74. Tsokas P, Grace EA, Chan P, Ma T, Sealfon SC, Iyengar R, Landau EM, Blitzer RD (2005) Local Protein Synthesis Mediates a Rapid Increase in Dendritic Elongation Factor 1A after Induction of Late Long-Term Potentiation. J Neurosci 25:5833–5843. doi: 10.1523/JNEUROSCI.0599-05.2005

75. Vargas KJ, Makani S, Davis T, Westphal CH, Castillo PE, Chandra SS (2014) Synucleins Regulate the Kinetics of Synaptic Vesicle Endocytosis. J Neurosci 34:9364–9376. doi: 10.1523/JNEUROSCI.4787-13.2014

76. Vizcaíno JA, Csordas A, del-Toro N, Dianes JA, Griss J, Lavidas I, Mayer G, Perez-Riverol Y, Reisinger F, Ternent T, Xu Q-W, Wang R, Hermjakob H (2016) 2016 update of the PRIDE database and its related tools. Nucleic Acids Res 44:D447–D456. doi: 10.1093/nar/gkv1145

77. Walker L, Stefanis L, Attems J (2019) Clinical and neuropathological differences between Parkinson's disease, Parkinson's disease dementia and dementia with Lewy bodies – current issues and future directions. J Neurochem jnc.14698. doi: 10.1111/jnc.14698

78. Wang X, Huang T, Bu G, Xu H (2014) Dysregulation of protein trafficking in neurodegeneration. Mol Neurodegener 9:31

79. Whittaker VP, Michaelson I, Kirkland RJA (1964) The separation of synaptic vesicles from nerve-ending particles (synaptosomes'). Biochem J 90:293

80. Wong YC, Krainc D (2017) α-synuclein toxicity in neurodegeneration: mechanism and therapeutic strategies. Nat Med 23:1–13. doi: 10.1038/nm.4269

81. Xu J, Wu X-S, Sheng J, Zhang Z, Yue H-Y, Sun L, Sgobio C, Lin X, Peng S, Jin Y, Gan L, Cai H, Wu L-G (2016) α-Synuclein Mutation Inhibits Endocytosis at Mammalian Central Nerve Terminals. J Neurosci Off J Soc Neurosci 36:4408–4414. doi: 10.1523/JNEUROSCI.3627-15.2016

82. Yang F, Demma M, Warren V, Dharmawardhane S, Condeelis J (1990) Identification of an actin-binding protein from Dictyostelium as elongation factor 1a. Nature 347:494–496. doi: 10.1038/347494a0

Figure legends:

Figure 1: Spine loss in PDGF-h-αS mice is the scientific background for FASS. A: Exemplary confocal images of apical tuft dendrites with spines (green arrowheads) in the somatosensory cortex of h-αS x GFP-M mice. Age-dependent spine loss in young adult h-αS mice occurs between 8 and 18 weeks of age. n = 5 mice per group, mean with s.e.m, Student‘s t-test; $^{**}p<0.01$, $^{***}p<0.001$; scale bar = 5µm. B: FASS workflow; synaptosomes were obtained from 12-week-old h-αS x VGLUT1^{VENUS} mice and purified using FASS. Validation was performed on mouse and human brain tissue. C: Western blot against GFP shows no differential expression of endogenous VGLUT1^{VENUS} levels in control and h-αS mice. D: sub-gating of particles according to their size and to VGLUT1^{VENUS} fluorescence during FASS. Fraction P3 represents VGLUT1^{VENUS} positive events. E: independent FASS experiments from individual mice show comparable enrichment in VGLUT1^{VENUS} particles.

Figure 2: Proteomic MS data reveals a set of 42 proteins with significantly different abundance in h-αS synaptosomes. A: graphic representation of protein hits according to log2(fold change) and –log10(p value). Gene names: Ap2a1 / -b1: AP-2 complex subunit alpha-1 / -beta1; eEF1A1: eukaryotic elongation factor 1 alpha-1; Mapt: microtubule associated protein tau; Ppp3r1: Calcineurin subunit B; Ndufs6: NADH dehydrogenase iron-sulfur protein 6; Nufv1: NADH dehydrogenase flavoprotein1; Rab1B / -3A: Ras-related protein Rab-1B / -3A; Rtn 1/-4: Reticulon 1 /-4; Syngr3: synaptogyrin 3; Stxbp1: Syntaxin-binding protein 1 (Munc18-1); Tuba4a: Tubulin alpha-4A; Tubb2a /-3 /-4a /-5: Tubulin beta-2A/-3/-4A/5. B: KEGG pathway enrichment highlights the involvement of related cellular and disease-related protein pathways. C: IntAct database analysis for the determination of the interacting proteomic network. The majority of proteins listed have eEF1A1 as interacting partner (see Supplementary Table S3).

Figure 3: eEF1A1 is reduced in synaptosomes of h-αS mice. A: Western blot of homogenates and S-synaptosomes. n = 3 mice per group, mean with s.e.m, Student‘s t-test; *p<0.05. B: Example quantification of individual FASS-synaptosomes. (b1) VGLUT1^{VENUS} fluorescence (green) was used to detect the volume of a synaptosome (delineated with white line). (b2) Immunofluorescence of the second marker (here eEF1A1 in magenta) was used to detect volume of associated marker (delineated with white line). (b3) Overlay of VGLUT1^{VENUS} and eEF1A1 immunofluorescence. (b4) Overlay of the detected synaptosome and the associated eEF1A1 positive structure. Scale bar = 1 µm. C: 48 randomly selected eEF1A1-positive synapses displayed as a gallery for control (c1) and h-αS (c2) mice; scale bar = 2 µm. D: cumulative frequency of eEF1A1/ VGLUT1^{VENUS} fluorescence signals; Kolmogorov-Smirnov test; ***p < 0.01. E: intensity signals from all FASS-synaptosomes quantified, as eEF1A1/ VGLUT1^{VENUS} ratios. F: mean eEF1A1/ VGLUT1^{VENUS} signals. n = 3 mice per group, mean with s.e.m, Student‘s t-test; **p<0.01. G: STED microscopy of eEF1A1 and VGLUT1^{VENUS} signals reveals the location of eEF1A1 at both pre- and postsynapses: arrows point to eEF1A1 positive structures excluded from the VGLUT1^{VENUS} positive presynapse, likely belonging to the postsynaptic compartment; scale bar = 1 µm.

Figure 4: eEF1A1 is reduced in the h-αS mouse cortex and correlated with a reduction in PSD95. A: Representative images of mouse somatosensory cortex stained for eEF1A1; scale bar = 50 µm. B: Top: maximum intensity projections of cortical layer I field of view. Bottom: magnified area from top panel illustrating spot detection (magenta). Scale bar = 10 µm. C: Cumulative distribution of the mean eEF1A1 intensity. The curves of h-αS mice show a strong left shift towards less intense values. D: Mean eEF1A1/VGLUT1^{VENUS} ratio of fluorescence intensity. E: Reduced density / µm of eEF1A1 positive spots in h-αS mice. F: Cumulative distribution of the mean PSD95 intensity. G: Mean PSD95 fluorescence intensity is reduced in h-

αS mice. H: Reduction of PSD95 spot density / µm in h-αS mice. n = 5 mice per group, mean with s.e.m., Student‘s t-test; *p<0.05, **p<0.01, ***p<0.001.

Figure 5: eEF1A1 expression is reduced in *post mortem* human neuropil of LBD patients. A: Western blot of cingulate cortex homogenate. B, C: eEF1A1 levels are similar in human cortex homogenates, PSD95 expression is reduced in advanced LBD (stage 5/6). n = 5 (control) and n = 6 (LBD), mean with s.e.m., Student’s t-test; *p<0.05. D: proteinase K-resistant deposits of αS are present as Lewy bodies (arrowhead) and Lewy neurites (arrows) in the cingulate gyrus of late-stage LBD. Image from the same brain as in E (LBD 5/6). E: Exemplary eEF1A1 staining in human cingulate gyrus from a control, mid-stage (Braak 3/4) and late-stage (Braak 5/6) LBD case, respectively. F: eEF1A1 staining intensity is reduced in the layer I of cingulate gyri of LBD brains. n = 9 (ctrl), n = 6 (LBD 3/4), n=12 (LBD 5/6), mean with s.e.m., Student‘s t-test; *p<0.05, **p<0.01. Scale bars = 20 µm.

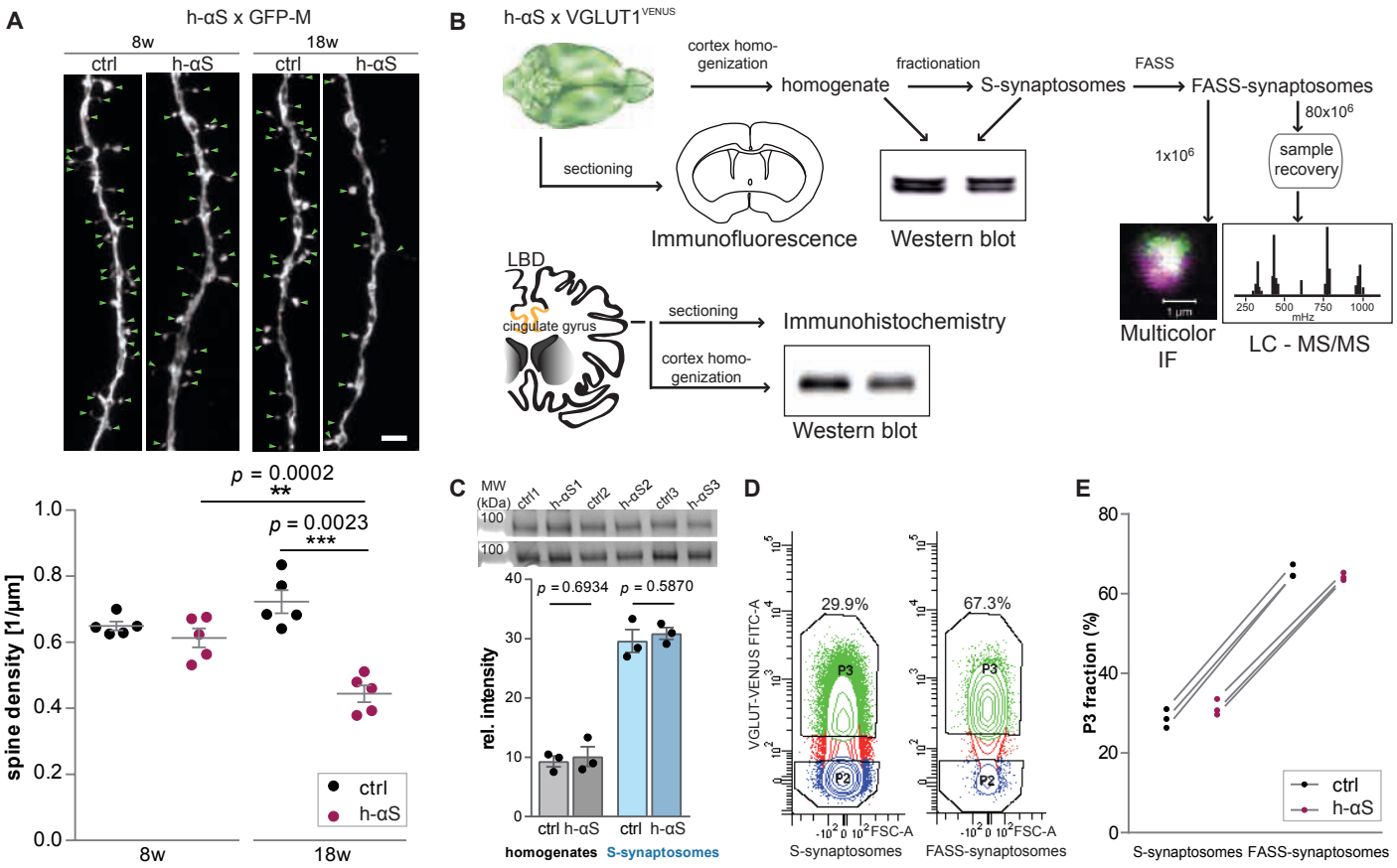
A
h-αS x GFP-M
8w
18w
ctrl
h-αS
ctrl
h-αS
p = 0.0002
**
p = 0.0023
***
spine density [1/µm]
1.0
0.8
0.6
0.4
0.2
0.0
ctrl
h-αS
8w
18w
B
h-αS x VGLUT1VENUS
cortex homo-genization
homogenate
fractionation
S-synaptosomes
FASS
FASS-synaptosomes
80x10^6
1x10^6
sample recovery
sectioning
Immunofluorescence
Western blot
LBD
cingulate gyrus
sectioning
Immunohistochemistry
cortex homo-genization
Western blot
Multicolor IF
LC - MS/MS
250
500
750
1000
mHz
1 µm
C
MW (kDa)
ctrl1
h-αS1
ctrl2
h-αS2
ctrl3
h-αS3
100
100
p = 0.6934
p = 0.5870
rel. intensity
40
30
20
10
0
ctrl h-αS
ctrl h-αS
homogenates
S-synaptosomes
D
29.9%
67.3%
P3
P2
P3
P2
VGLUT-VENUS FITC-A
FSC-A
FSC-A
S-synaptosomes
FASS-synaptosomes
E
P3 fraction (%)
80
60
40
20
0
ctrl
h-αS
S-synaptosomes
FASS-synaptosomes

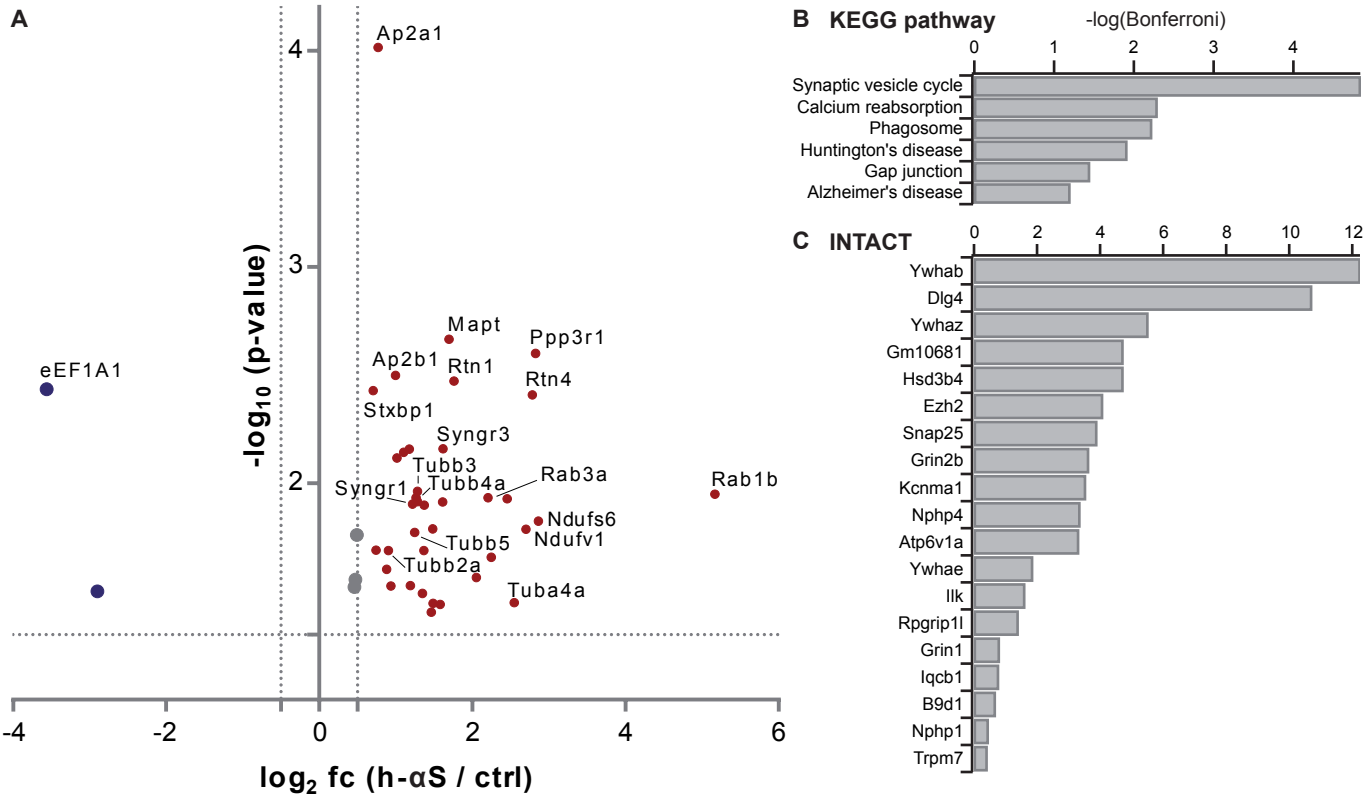
A
Ap2a1
Mapt
Ppp3r1
Ap2b1
Rtn1
Rtn4
eEF1A1
Stxbp1
Syngr3
Tubb3
Syngr1
Tubb4a
Rab3a
Rab1b
Ndufs6
Ndufv1
Tubb5
Tubb2a
Tuba4a
-log10 (p-value)
log2 fc (h-αS / ctrl)
B KEGG pathway
-log(Bonferroni)
Synaptic vesicle cycle
Calcium reabsorption
Phagosome
Huntington's disease
Gap junction
Alzheimer's disease
C INTACT
Ywhab
Dlg4
Ywhaz
Gm10681
Hsd3b4
Ezh2
Snap25
Grin2b
Kcnma1
Nphp4
Atp6v1a
Ywhae
Ilk
Rpgrip1l
Grin1
Iqcb1
B9d1
Nphp1
Trpm7

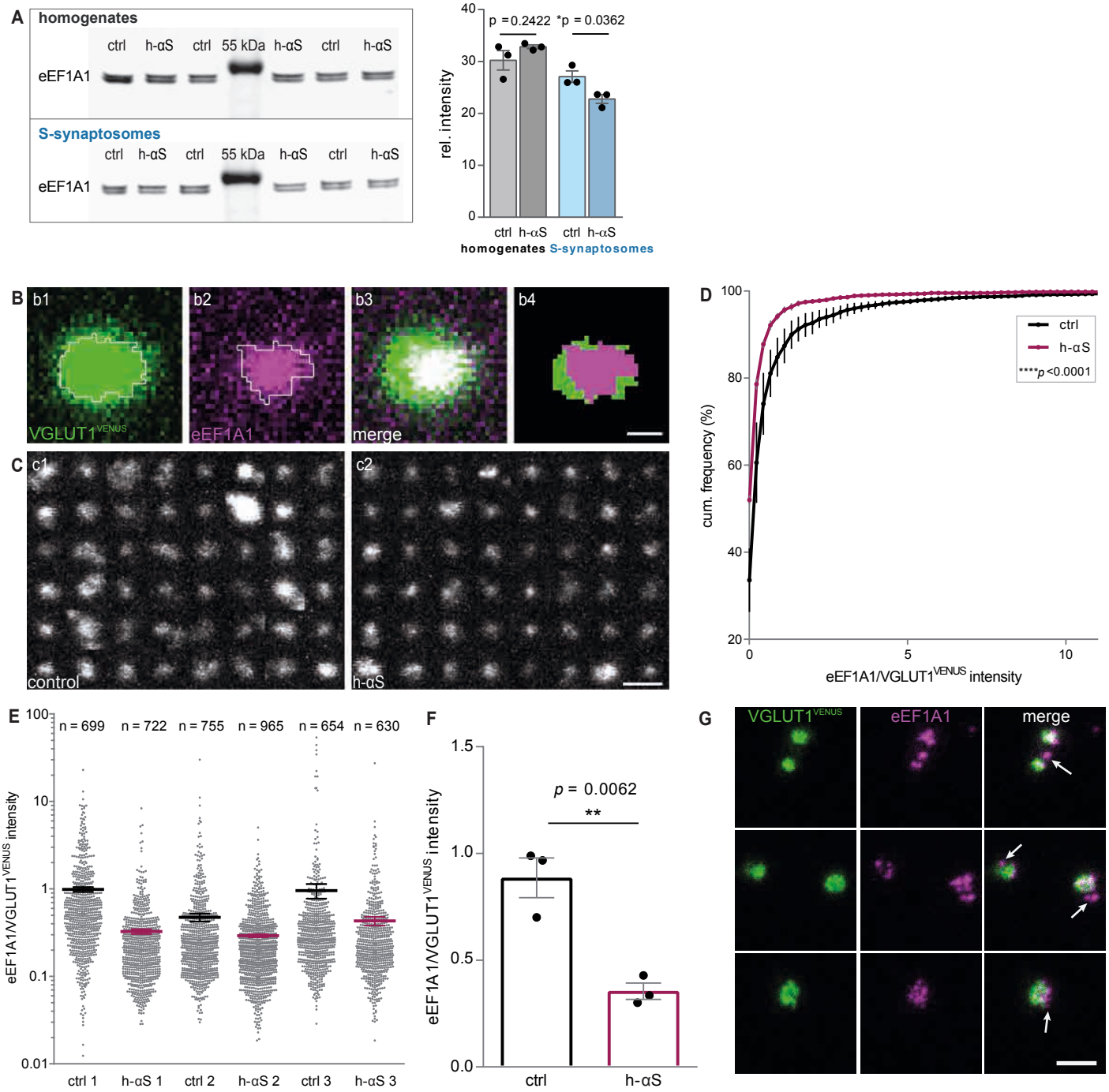
A
homogenates
ctrl h-αS ctrl 55 kDa h-αS ctrl h-αS
eEF1A1
S-synaptosomes
ctrl h-αS ctrl 55 kDa h-αS ctrl h-αS
eEF1A1
rel. intensity
p = 0.2422
*p = 0.0362
ctrl h-αS ctrl h-αS
homogenates S-synaptosomes
B
b1
b2
b3
b4
VGLUT1VENUS
eEF1A1
merge
C
c1
c2
control
h-αS
D
cum. frequency (%)
ctrl
h-αS
****p <0.0001
eEF1A1/VGLUT1VENUS intensity
E
n = 699 n = 722 n = 755 n = 965 n = 654 n = 630
eEF1A1/VGLUT1VENUS intensity
ctrl 1 h-αS 1 ctrl 2 h-αS 2 ctrl 3 h-αS 3
F
p = 0.0062
**
eEF1A1/VGLUT1VENUS intensity
ctrl h-αS
G
VGLUT1VENUS
eEF1A1
merge

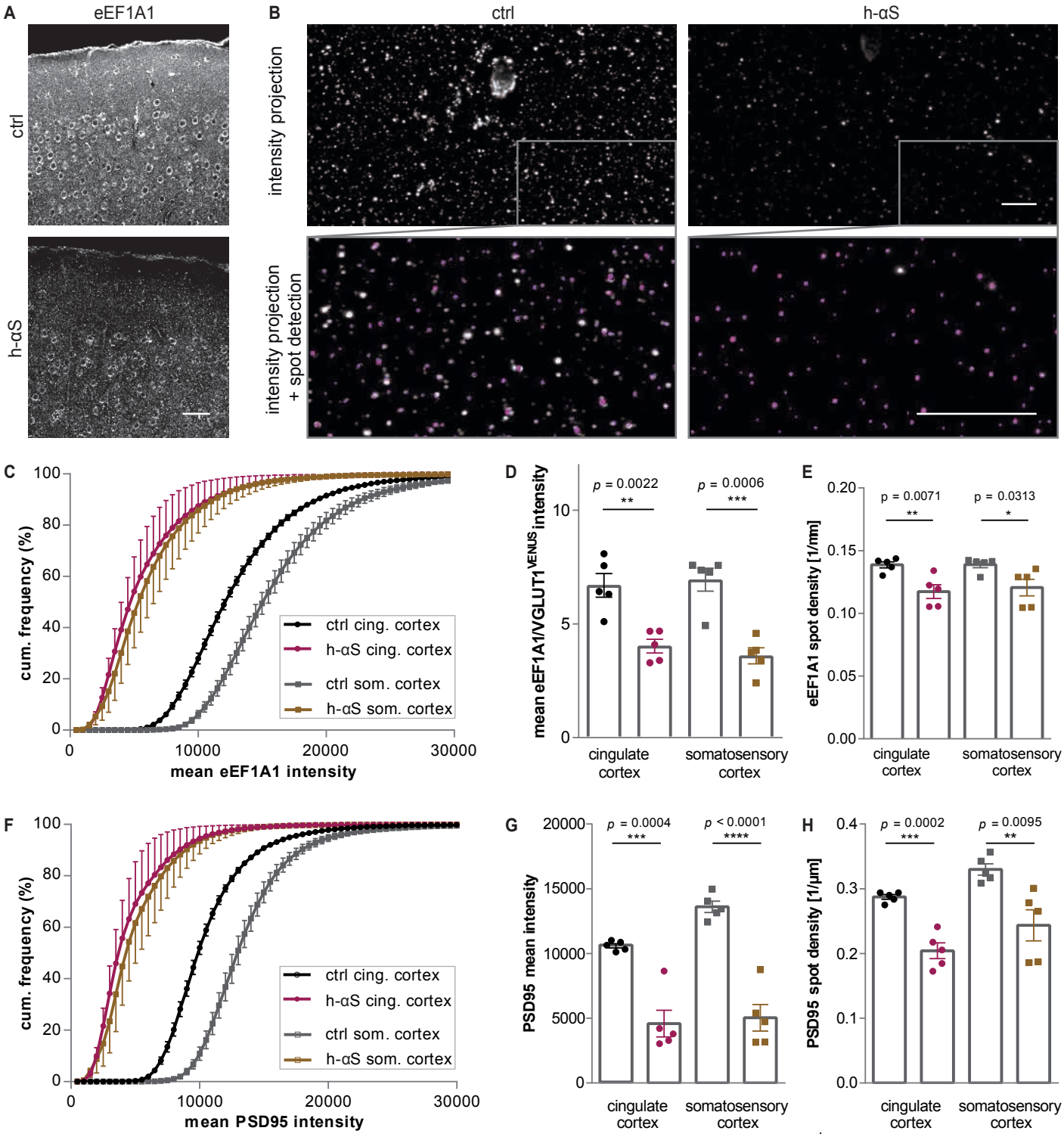
A
eEF1A1
ctrl
h-αS
B
ctrl
h-αS
intensity projection
intensity projection
+ spot detection
C
cum. frequency (%)
mean eEF1A1 intensity
ctrl cing. cortex
h-αS cing. cortex
ctrl som. cortex
h-αS som. cortex
D
mean eEF1A1/VGLUT1VENUS intensity
p = 0.0022
**
p = 0.0006
***
cingulate cortex
somatosensory cortex
E
eEF1A1 spot density [1/mm]
p = 0.0071
**
p = 0.0313
*
cingulate cortex
somatosensory cortex
F
cum. frequency (%)
mean PSD95 intensity
ctrl cing. cortex
h-αS cing. cortex
ctrl som. cortex
h-αS som. cortex
G
PSD95 mean intensity
p = 0.0004
***
p < 0.0001
****
cingulate cortex
somatosensory cortex
H
PSD95 spot density [1/µm]
p = 0.0002
***
p = 0.0095
**
cingulate cortex
somatosensory cortex

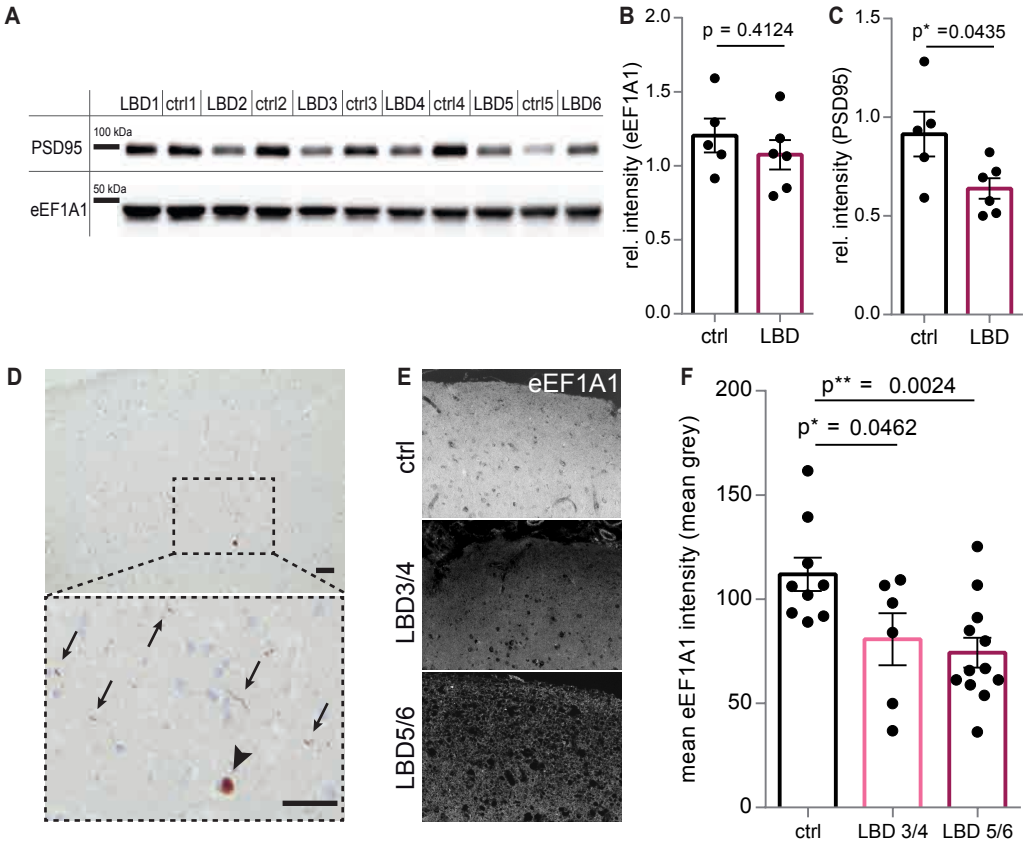
A
LBD1 ctrl1 LBD2 ctrl2 LBD3 ctrl3 LBD4 ctrl4 LBD5 ctrl5 LBD6
PSD95
100 kDa
eEF1A1
50 kDa
B
p = 0.4124
rel. intensity (eEF1A1)
2.0
1.5
1.0
0.5
0.0
ctrl
LBD
C
p* =0.0435
rel. intensity (PSD95)
1.5
1.0
0.5
0.0
ctrl
LBD
D
E
eEF1A1
ctrl
LBD3/4
LBD5/6
F
p** = 0.0024
p* = 0.0462
mean eEF1A1 intensity (mean grey)
200
150
100
50
0
ctrl
LBD 3/4
LBD 5/6